Evaluation of Fe-Doped CGO Electrolyte for Application in IT-SOFCs

ECS Transactions, 91 (1) 1209-1216 (2019)
10.1149/09101.1209ecst ©The Electrochemical Society

Evaluation of Fe-doped CGO Electrolyte for Application in IT-SOFCs

M. Machado, L. P. R. Moraes, L. N. Rodrigues, M. Tabanez, M. Ferrazoli, and F. C. Fonseca

Nuclear and Energy Research Institute, IPEN-CNEN/SP, University of São Paulo, São Paulo, Brazil

A challenge encountered with intermediate temperature solid oxide fuel cells (IT-SOFCs) is lowering the densification temperature of the doped ceria electrolyte and improving its ionic conductivity. Ceria doped with 10 mol% gadolinium oxide and 0, 1, 5 mol% iron oxide were synthesized by a low temperature precipitation route based on hexamethylenetetramine as the precipitating agent. The as-synthesized precursors are nanocrystalline powders with a homogeneous morphology. Co-doping with Fe^{3+} changes the sintering behaviour of the doped cerium oxide and favours densification at lower temperatures. Through a comprehensive elementary, structural, microstructural and electrochemical analysis of the co-doped cerium oxide, it was established the doping mechanism of Fe^{3+} and its effect on the bulk and grain boundary conductivities. The overall aim is to evaluate its suitability for application as an electrolyte in IT-SOFC applications.

Introduction

Cerium oxide has the capacity to display an oxygen nonstoichiometry ($CeO_{2-\delta}$) due to the double valence state of ceria ($Ce^{+3/+4}$), which results in oxygen vacancies, n-type conductivity, and phase changes. The stability of ceria can, however, be increased by doping it with a trivalent element such as gadolinium. This doping further increases the number of oxygen ion vacancies granting the material high ionic conductivity, fundamental for many solid-state electrochemistry applications, including solid oxide fuel cells (SOFCs). Cerium oxide doped with 10 mol% gadolinium (CGO) has been widely studied for its application as an electrolyte in intermediate temperatures solid oxide fuels cells (IT-SOFCs). 10 mol% CGO exhibits a higher ionic conductivity than the usual yttria stabilized zirconia (YSZ) electrolyte at moderate temperatures, between 600 °C and 800 °C (1-4).

Ceria based oxides are difficult to densify, requiring a high sintering temperature, around 1500 °C to obtain a fully dense ceramic body. The high sintering temperature entails high energy costs and hinders co-firing the electrolyte with other components of the cell. Several techniques have been investigated to improve the sintering of cerium oxides, generally involving the control of the precursor ceramic powders. Synthesis approaches using wet chemistry result in oxide powders with a high specific surface area and, consequently, a high activity towards densification mechanisms (5,6). Densification temperature can further be reduced by the addition of a sintering aid such as a transition metal oxide (7-10).

However, doping with a transition metal oxide can lead to an increase in electronic conductivity, which is prohibitive in an electrolyte because it can lead to an internal short circuit reducing the output performance of the fuel cell. In an atmosphere of low oxygen activity and high temperature there is an increase in electronic conductivity, such is the condition of the fuel side of the SOFC. Consequently, the necessity to evaluate the electronic activity of the ceria electrolyte when doped with transition metal oxide. This electronic conductivity can be estimated from the dependence of conductivity on the oxygen partial pressure (11,12).

In this study we report the preparation of nanocrystalline highly reactive CGO doped with 0, 1 and 5 mol% Fe^{3+} electrolytes via a simple, low temperature aqueous homogeneous precipitation method. The purpose of adding Fe^{3+} is to lower sintering temperature and improve electrolyte performance for its potential application in IT-SOFC. The low temperature sintered electrolytes were characterized by their microstructures and electrical conductivities.

Experimental

Ceria doped with 10 mol % gadolinium oxide and 0, 1, 5 mol% iron oxide powder was synthesized using a homogeneous precipitation method. An aqueous solution of cerium (III) nitrate ($Ce(NO_3)_3 \cdot 6H_2O$, 99%), gadolinium (III) nitrate ($Gd(NO_3)_3 \cdot 6H_2O$, 99.9%) and iron (III) nitrate ($Fe(NO_3)_3 \cdot 9H_2O$, 98%), all purchased by Sigma Aldrich, was heated to 85 °C under continuous stirring. Hexamethylenetetramine (HMT, 99%, Sigma Aldrich) was added to the aqueous solution so that precipitation occurred, and the stirring was maintained for 3 h at 85 °C. The precipitate was washed in the centrifuge and dried at 100 °C for 12 h and calcined at 500 °C.

After calcination, the powder obtained was grinded at a planetary ball mill to break soft agglomerates. Zirconia balls (⌀ < 5mm) were used as the grinding media. Energy-dispersive X-ray fluorescence spectrometer, EDX-720 Shimadzu, was used to obtain a semi-quantitative elementary analysis of the synthesized materials. X-ray diffraction analyses were performed using the Miniflex II diffractometer with CuKα radiation (0.15406 nm). Mean crystallite sizes were calculated using Scherrer's formula for peaks in the 2θ range from 20° to 80°. Cylindrical pellets were prepared by uniaxial pressing for dilatometry (TMA) analyses (Setaram Labsys), between ambient temperature and 1400 °C with a heating rate of 10 °C/min under synthetic air flow.

The microstructure of the fractured surfaces of sintered samples was studied using a field emission gun scanning electron microscope FEG-SEM (JEOL, JSM-6701F). The electrical properties of the material were analysed by impedance spectroscopy measurements of the sintered samples from the temperature range of 300 °C - 800 °C. The *p*O2 was controlled by an yttria-stabilized zirconia oxygen pump and sensor (Setnag Gen'air) with injection of synthetic air, hydrogen (4 %, balanced with Argon) and nitrogen at controlled flow rates (~20 ml/min). The impedance measurements were performed by the Solartron frequency analyser (SI 1260), with frequency ranging from 10 MHz to 1 Hz and ac amplitude of 100 mV.

Results and Discussion

The semi-quantitative elementary analyses carried out by the X-ray fluorescence (XRF) results indicated a good agreement between nominal (1 and 5 mol%) and measured (1 and 4 mol%) values of Fe_2O_3 content. Zirconia was found in some samples (< 5 mol%), possibly as a result of the milling step carried out with zirconia grinding medium.

The X-ray diffractograms (XRDs) (Figure 1) of the calcined powders of CGO doped with iron oxide shows diffraction peaks corresponding the ceria fluorite phase (JCPDS 75-0161). Mean crystallite sizes were calculated and were of ca. 10 nm for all samples. The precipitation agent HMT controls the rate of the precipitation, it hydrolyzes slowly to produce formaldehyde and ammonia changing the pH evenly throughout the solution to produce homogeneous ultrafine particles (13). The calculated average lattice parameters were of 5.41, 5.40 and 5.39 Å for the 0, 1 and 5 mol% Fe^{3+}, respectively. The shift in lattice parameter might indicate that some of the Fe^{3+} has entered the crystal structure as the radius of the Fe ion is smaller than that of the Ce and Gd ions causing a small XRD shift towards higher angles with the addition of Fe^{3+} (14).

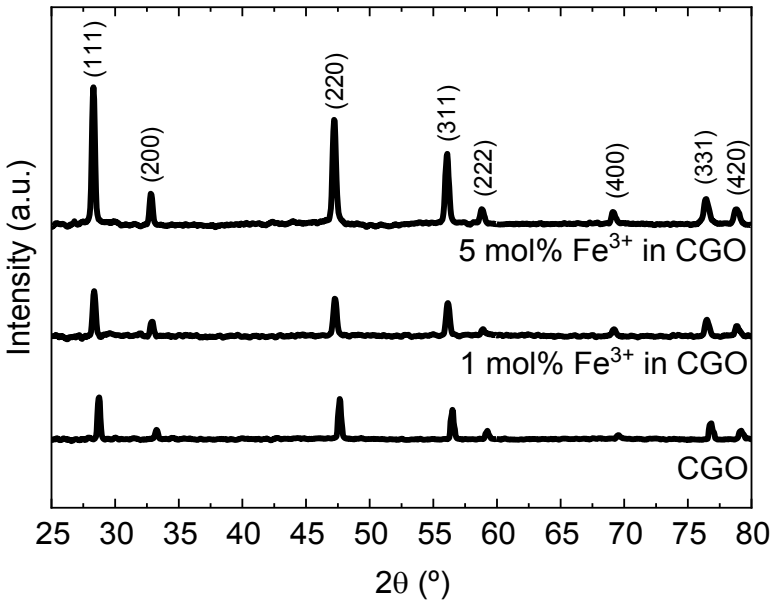

Figure 1. X-ray patterns of 0, 1 and 5 mol% Fe^{3+} doped CGO powders after calcination at 500 °C.

Figure 2 shows the densification profile and the densification rate curves for the studied samples. The relative green densities (ρ_0) of the samples were of ca. 38 % for both CGO and 1 mol% Fe^{3+}, and 35 % for 5 mol% Fe^{3+} doped CGO. Densification develops at low temperature and a more significant densification starts at ~800 °C for the Fe-doped sample, whereas CGO has a higher onset densification (~1000 °C). With increasing temperature, densification increases rapidly and sample 1 mol% Fe^{3+} is the only to clearly reach final sintering stage at T<1400 °C corresponding to reminiscent

porosity elimination and grain growth (15). Interestingly, all samples exhibit two well-defined densification activity maxima as shown in the dρ/dT curve (Figure 2. (b)). CGO has a two-step densification profile, where the first process at lower temperature (~1100 °C) shows higher activity and is related to the surface diffusion resulting in particle agglomeration and particle-to-particle neck formation. The second process at ~1250 °C is less intense and is due primarily to lattice diffusion-limited solid-state diffusion process. Such profile is consistent with previous results on high surface area CGO nanocrystals (16) and indicates limited grain growth. Doping CGO with 1 mol% and 5 mol% Fe^{3+} results in a different sintering activity as compared to CGO. For samples with 1 and 5 mol% Fe^{3+} the first maximum becomes less intense and it is displaced towards lower temperatures with increasing Fe^{3+} content, indicating that surface diffusion mechanism is enhanced by the dopant. On the other hand, the second maximum shows the highest activity and occurs at a higher temperature (T ~1300°C) for both Fe-doped samples than for CGO, suggesting a higher activation energy and possibly more intense grain growth for Fe-doped samples. In order to further study the effect of Fe doping on CGO we have chosen to sinter samples initially at a temperature close to the maximum activity of the CGO sample, i.e., T=1200°C. The measured hydrostatic apparent densities of CGO samples sintered at 1200 °C was 72%, 90% and 85% for samples with 0, 1 and 5 mol% Fe^{3+}, respectively.

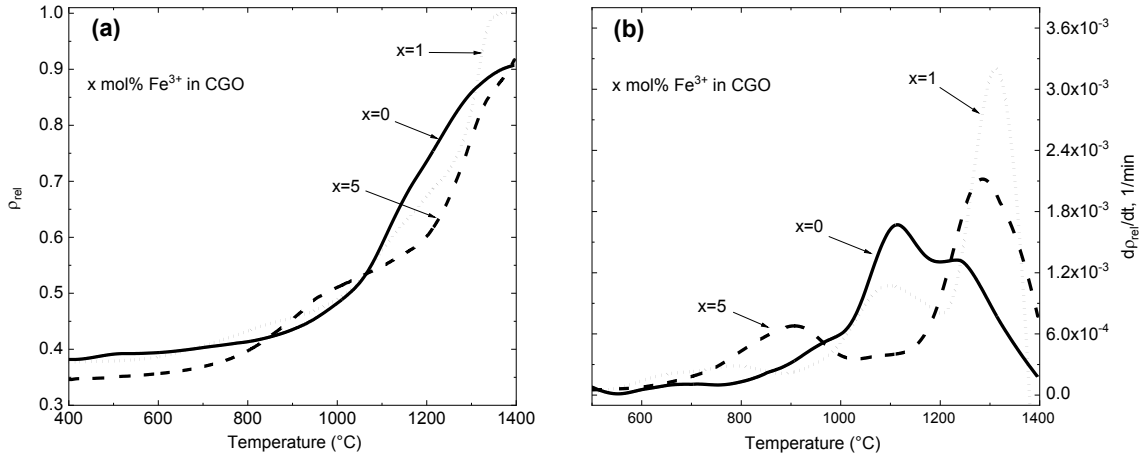

Figure 2. (a) Densification profiles and (b) rate of densification profiles of calcined powder with 0, 1 and 5 mol% Fe^{3+} in CGO.

The SEM images of the fractured surfaces of samples sintered at 1200 °C are shown in Figure 3. The observed microstructures are in accordance with the calculated densities and with the densification processes discussed based on dilatometry runs (Figure 2). CGO without sintering aid exhibits a porous structure with sub-micron grain size. Adding Fe^{3+} to CGO enhances the densification and promotes grain growth as observed for samples with 1 and 5 mol% Fe^{3+} CGO.

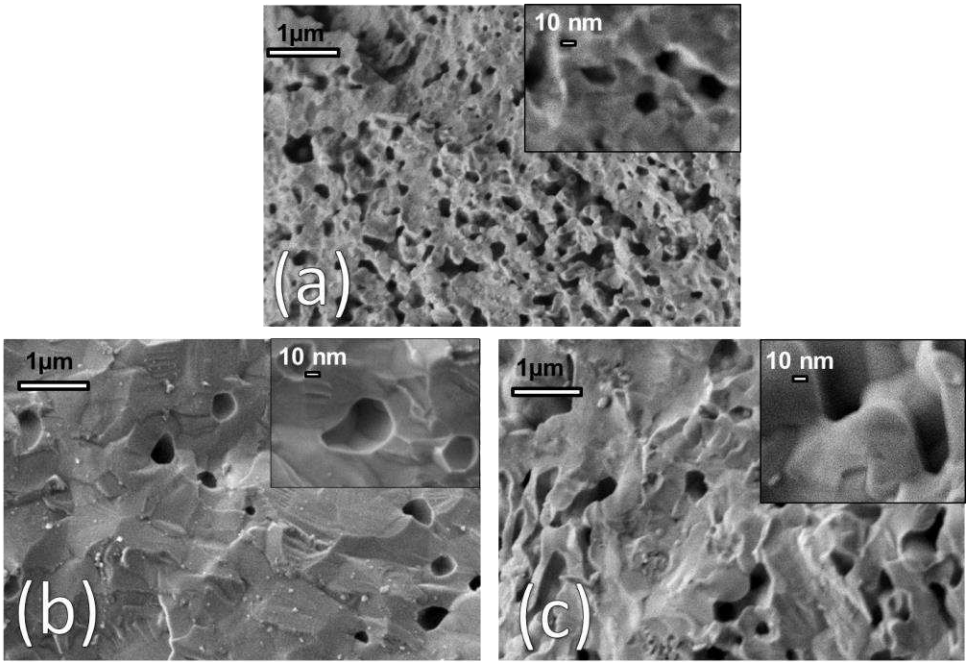

Figure 3. SEM images of (a) the fractured CGO, (b) 1 mol% Fe^{3+} in CGO and (c) 5 mol% Fe^{3+} in CGO sintered at 1200 °C.

Impedance spectroscopy data at 350 °C are shown as Nyquist plots in Figure 4. The impedance diagrams show two components related to the CGO samples. The high frequency arc develops at ~1 MHz at 350 °C and it is related to the bulk conductivity. A much larger semi-circle observed in the 10^2-10^3 Hz frequency range is due to blocking of charge carriers at the grain boundary and pores. The spike observed at low frequency is due to the electrode reactions. The blocking resistance due to both pores and grain boundaries predominates over the bulk resistance, thus being the main component of the electrical resistivity. All samples exhibit similar bulk resistivity indicating that Fe doping has less effect in such component, whereas the blocking semi-circle is much larger for the sample without Fe^{3+}, in accordance with its lower density.

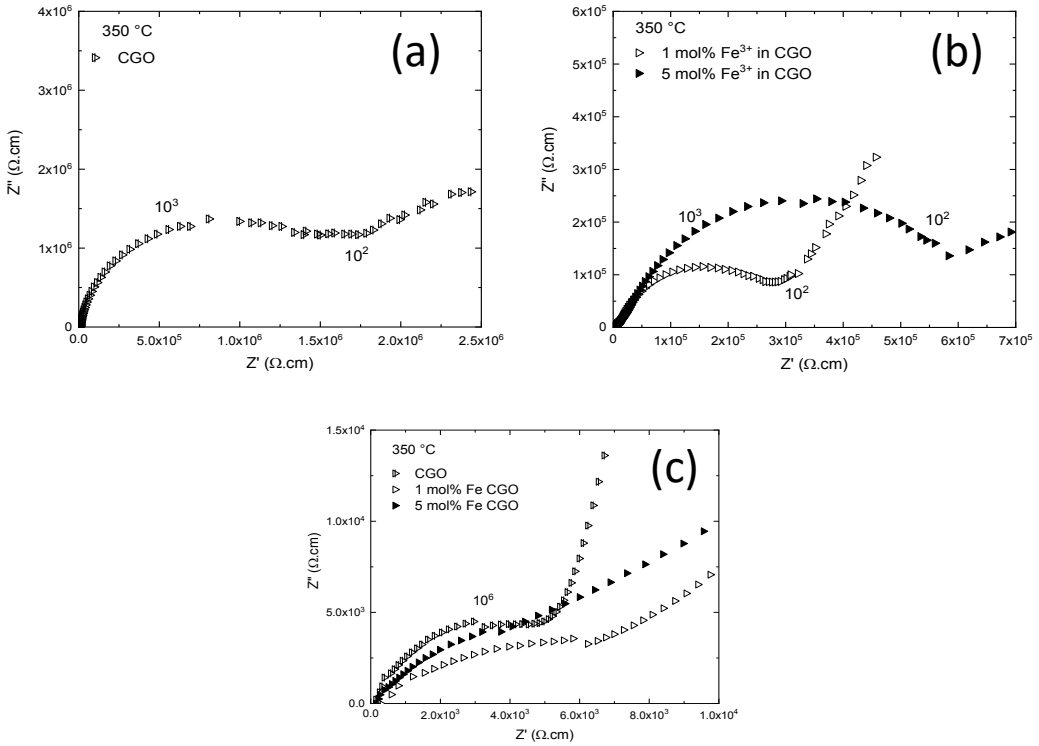

Figure 4. Nyquisit plots measured at 350 °C of (a) CGO, (b) 1 and 5 mol% Fe^{3+} doped-CGO, and (c) expanded view of high-frequency range of all samples.

Arrhenius plots of total conductivity and bulk conductivity extracted form the impedance diagrams measured in the temperature range 300 - 800 °C are shown in Figure 5. All samples exhibit thermally activated conductivity with typical activation energy values of oxygen ion conductors. The sample showing the lowest conductivity is CGO due to the large fraction of pores, as expected. An improvement in the ionic conductivity is observed by the addition of 1 mol% Fe^{3+}. However, further increasing the Fe^{3+} content, as in sample 5 mol% Fe^{3+}, decreases the total conductivity as porosity and possibly a Fe-rich phase is likely to segregate at the grain boundary. The value of the bulk conductivity was deconvoluted in the 300-450 °C temperature range. The bulk conductivity of all samples is comparable, and samples exhibit the typical activation energy observed for ceria-based electrolytes (0.7 eV). It is evident that the main differences in the total conductivity of the samples is due to the charge transport at grain boundaries, which have a higher activation energy (1.2 eV).

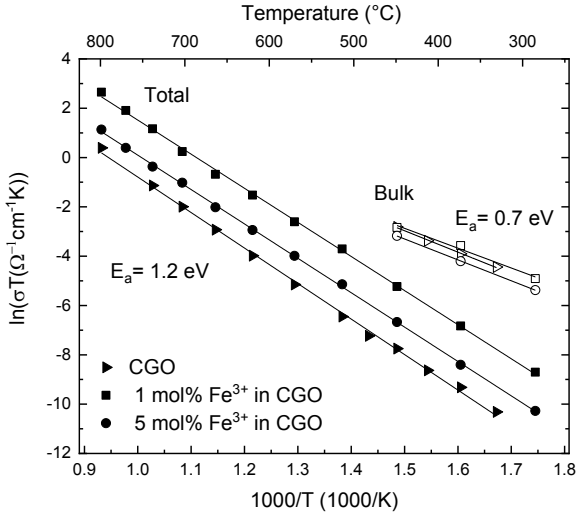

Figure 5. Arrhenius plots of the total and bulk conductivities in air of 0, 1 and 5 mol% Fe^{3+} in CGO.

Further analysis of the electrical transport of Fe-doped CGO samples was carried out by varying the oxygen partial pressure during the impedance measurements. pO_2-dependent impedance measurements are helpful to evaluate if the addition of Fe^{3+} as a sintering aid increases the electronic conductivity of the CGO. The total conductivity was extracted from the of impedance data measured at different pO_2 at 400 °C, as shown in Figure 6. It is observed that sample with 1 mol% Fe^{3+} CGO exhibits higher ionic conductivity in the pO_2 range 10^{-5} - 1 atm, whereas for measurements carried out under hydrogen (4%), corresponding to pO_2= 10^{-24} atm, the 5 mol% Fe^{3+} CGO exhibits a higher conductivity. The higher conductivity of the sample with the highest Fe^{3+} content may be associated with the rise of the electronic conductivity component in such materials, indicating that Fe-rich phase is possibly segregated in grain boundaries. Further analyses to unveil the influence of Fe-doping on the microstructural and electrical properties of CGO are underway.

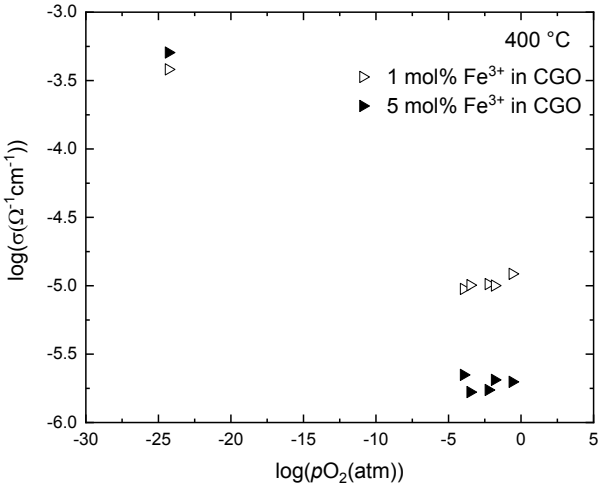

Figure 6. Total conductivity as a function of pO_2 at 400 °C for 1 and 5 mol% Fe^{3+} in CGO.

Conclusion

Single-phase Fe-doped CGO nanocrystals were synthesized at mild temperature by a homogenous precipitation method. The Fe^{3+} ions were shown to be an effective sintering aid. Samples with 1 mol% of Fe^{3+} exhibit apparent density (90%) approaching the requirements for a SOFC electrolyte at a relatively lower sintering temperature (1200 °C) as compared to CGO without sintering aid. The addition of Fe^{3+} increased the activation energy for lattice diffusion during sintering resulting in larger grain sizes than the CGO sample. The higher density of CGO with 1 mol% of Fe^{3+} favors higher conductivity values than the undoped sample and the one with a higher Fe^{3+} amount, such as 5 mol%. It was shown that addition of 5 mol% Fe^{3+} to CGO was less effective on assisting the sintering process and a higher amount of Fe^{3+} increased the electronic component of the total electrical conductivity at low oxygen partial pressure.

Acknowledgments

The authors are thankful for the support of the Brazilian agencies CAPES, CNPq, CNEN and FAPESP (2016/07156-4, 2017/11937-4, 2014/09087-4, 2014/50279-4).

References

1. A. Atkinson, *Solid State Ion*., **95**, 249 (1997).
2. A. Atkinson, S. Barnett, R. J. Gorte, J. T. S. Irvine, A. J. McEvoy, M. Mogensen, S. C. Singhal, and J. Vohs, *Nat. Mater*., 3, 17 (2004).
3. H. Inaba, *Solid State Ion*., **83**, 1 (1996).
4. B. Steele, *Solid State Ion.*, **129**, 95 (2000).
5. A. Sin, *Solid State Ion.*, **175**, 361 (2004).
6. J.-G. Cheng, S.-W. Zha, J. Huang, X.-Q. Liu, and G.-Y. Meng, *Mater. Chem. Phys*., **78**, 791 (2003).
7. M.-F. Han, S. Zhou, Z. Liu, Z. Lei, and Z.-C. Kang, *Solid State Ion*., **192**, 181 (2011).
8. A. K. Baral, H. P. Dasari, B.-K. Kim, and J.-H. Lee, *J. Alloys Compd.,* **575**, 455 (2013).
9. J. Nicholas and L. Dejonghe, *Solid State Ion*., **178**, 1187 (2007).
10. Y. Zheng, M. Zhou, L. Ge, S. Li, H. Chen, and L. Guo, J. *Alloys Compd*., **509**, 546 (2011).
11. S. Wang, T. Kobayashi, M. Dokiya, and T. Hashimoto, *J. Electrochem. Soc.,* **147**, 3606 (2000).
12. C. B. Gopal and S. M. Haile*, J Mater Chem A*, **2**, 2405 (2014).
13. P.-L. Chen and I.-W. Chen, *J. Am. Ceram. Soc.*, **76**, 1577 (1993).
14. Z. Wang, Y. Zeng, C. Li, Z. Ye, L. Cao, and Y. Zhang, *Ceram. Int.*, **44**, 10328 (2018).
15. V. Esposito, A. Kabir, M. Rosa, N. V. Nong, T. S. Rodrigues, L. N. Rodrigues, M. Machado, L. P. R. Moraes, D. Marani, and F. C. Fonseca, *Cryst. Eng. Commun*., doi: (Accepted Manuscript).
16. V. Esposito, D. W. Ni, Z. He, W. Zhang, A. S. Prasad, J. A. Glasscock, C. Chatzichristodoulou, S. Ramousse, and A. Kaiser, *Acta Mater*., **61**, 6290 (2013).